Geophysical Research Letters®

RESEARCH LETTER
10.1029/2021GL094104

Terrestrial Water Storage Anomalies Emphasize Interannual Variations in Global Mean Sea Level During 1997–1998 and 2015–2016 El Niño Events

Yan-Ning Kuo[1], Min-Hui Lo[1], Yu-Chiao Liang[1,2,3], Yu-Heng Tseng[4], and Chia-Wei Hsu[5]

[1]Department of Atmospheric Sciences, National Taiwan University, Taipei, Taiwan, [2]Lamont-Doherty Earth Observatory, Columbia University, Palisades, NY, USA, [3]Woods Hole Oceanographic Institution, Woods Hole, MA, USA, [4]Institute of Oceanography, National Taiwan University, Taipei, Taiwan, [5]Department of Atmospheric Science, Colorado State University, Fort Collins, CO, USA

Abstract Interannual variations in global mean sea level (GMSL) closely correlate with the evolution of El Niño-Southern Oscillation. However, GMSL differences occur in extreme El Niños; for example, in the 2015–2016 and 1997–1998 El Niños, the peak GMSL during the mature stage of the former (9.00 mm) is almost 2.5 times higher than the latter (3.72 mm). Analyses from satellite and reanalysis data sets show that the disparity in GMSL is primarily due to barystatic (ocean mass) changes. We find that the 2015–2016 event developed not purely as an Eastern Pacific El Niño event but with Central Pacific (CP) El Niño forcing. CP El Niños contribute to a stronger negative anomaly of global terrestrial water storage and subsequent higher barystatic heights. Our results suggest that the mechanism of hydrology-related interannual variations of GMSL should be further emphasized, as more CP El Niño events are projected to occur.

Plain Language Summary The global mean sea level (GMSL) varies at year-to-year timescale because of El Niño-Southern Oscillation, and GMSL is usually higher than normal during El Niños. The top two strongest El Niños in the past 30 years were the 1997–1998 and 2015–2016 events, whose strengths were similar, but the peak of GMSL in 2015–2016 was 2.5 times higher than that in 1997–1998. We analyze satellite and observation-based data sets with global coverage to show that the difference of GMSL mainly came from the increasing ocean water mass associated with decreasing land water storage. The higher sea level in the 2015–2016 El Niño was because the event was forced from the midlatitude atmosphere, established by the Central Pacific El Niño, instead of a pure tropical forced Eastern Pacific El Niño. The different El Niño types make different teleconnections affect land water storage, which is critical for global sea level variation.

Key Points:

- Variations of global mean sea level (GMSL) in two extreme El Niño events during the altimetry era are mainly due to barystatic differences
- Higher terrestrial water storage (TWS) anomalies during typical Eastern Pacific (EP) El Niño cause lower barystatic variations in the 1997–1998 event
- 2015–2016 and 1997–1998 El Niños were different in partitioning of their Central Pacific/EP forcings, leading to different TWS and corresponding GMSL

Supporting Information:

Supporting Information may be found in the online version of this article.

Correspondence to:

M.-H. Lo,
minhuilo@ntu.edu.tw

Citation:

Kuo, Y.-N., Lo, M.-H., Liang, Y.-C., Tseng, Y.-H., & Hsu, C.-W. (2021). Terrestrial water storage anomalies emphasize interannual variations in global mean sea level during 1997–1998 and 2015–2016 El Niño events. *Geophysical Research Letters*, *48*, e2021GL094104. https://doi.org/10.1029/2021GL094104

Received 27 APR 2021
Accepted 24 AUG 2021

1. Introduction

Global mean sea level (GMSL) informs climate variations: sea level rise since the beginning of the 20th century is indicated by increasing ocean heat content (OHC) and melting glacial ice (Cheng et al., 2019; Church et al., 2011; Hamlington, Fasullo, et al., 2019; Nerem et al., 2018). However, the rising trend in GMSL can be obscured by climate variabilities at various timescales, particularly the interannual one. Interannual variations in GMSL are dominated by El Niño-Southern Oscillation (ENSO) (e.g., Cazenave et al., 2012; Fasullo & Nerem, 2016; Gregory et al., 2013; Hamlington, Cheon, et al., 2019; Hamlington et al., 2020; Leuliette, 2015; Nerem et al., 2010). GMSL is manifested as a high correlation coefficient of 0.73 to the ENSO index during the 2005–2015 period (Piecuch & Quinn, 2016). Despite such a close GMSL-ENSO interannual relationship, the temporal features of GMSL could be distinct in one extreme ENSO event from another. For example, the peak strength of anomalous GMSL in extreme 2015–2016 El Niño was doubled than that in 1997–1998 extreme event (Figure 1a), but the reason for this remains unclear.

Sea level variations can be decomposed into steric (both the heat content and salinity changes) and barystatic (ocean mass) changes. The Earth's water balance is approximately a closed system at the interannual timescale; therefore, with the assumption that atmospheric water mass is relatively negligible at a monthly mean basis as the residence time of water vapor in the atmosphere is within 8–10 days (Ent & Tuinenburg, 2017), the interannual variation in barystatic sea level is a result of changes in terrestrial water storage

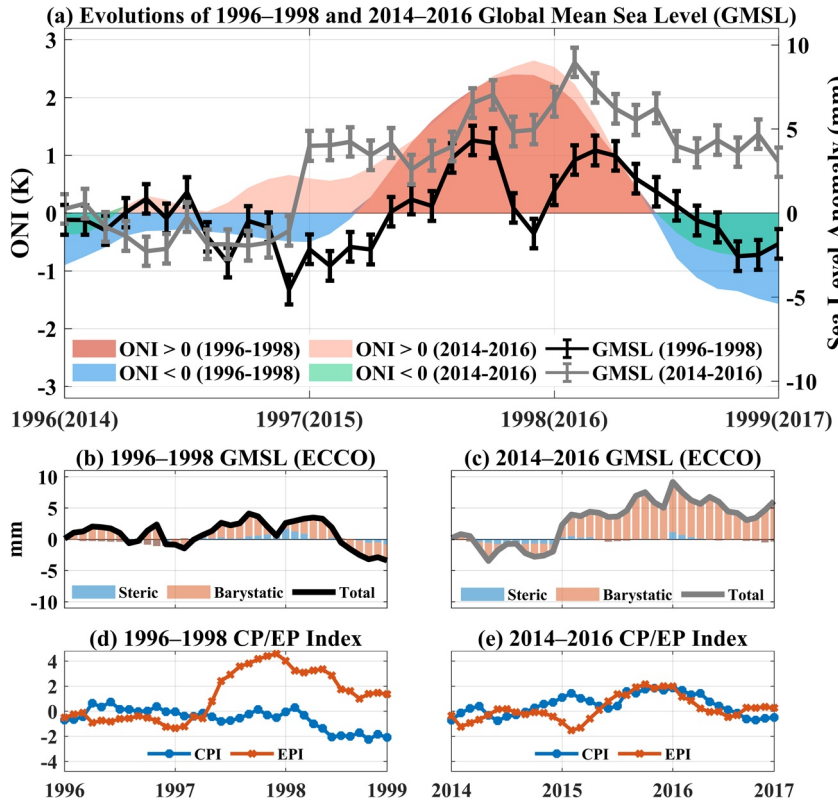

Figure 1. (a) Altimetry-observed global mean sea level (GMSL) in 1996–1998 and 2014–2016 overlaid with Oceanic Niño Index (ONI) strength shading (crimson and blue for 1996–1998; light red and green for 2014–2016). Error bars are the 90% confidence interval of standard deviation by the method in Section S2. Time series of sea level anomalies in (b) 1996–1998 and (c) 2014–2016 from Estimating the Circulation and Climate of the Ocean version 4 (ECCOv4r4): steric-plus-barystatic height (black line), steric height (blue bar), and barystatic height (red bar). Steric heights from ECCOv4r4 were derived according to Gill and Niller (1973). The barystatic heights from ECCOv4r4 are derived from the calculation of ocean bottom pressure with global mean air pressure removed (OBPNOPAB). Time series of Eastern Pacific (EP) indices and Central Pacific (CP) indices for (d) 1996–1998 and (e) 2014–2016.

(TWS). Following Equations 1 and 2 in Llovel et al. (2011) (also see Wada et al., 2016) based on land hydrological budget framework, we can formulate the TWS variations as:

$$\Delta M_{\text{ocean}} \fallingdotseq -\Delta M_{\text{TWS}} = -\left(P_{\text{land}} - E_{\text{land}} - R_{\text{land}}\right) \quad (1)$$

where Δ means the difference in each month, P_{land} is global-averaged land precipitation, E_{land} is global-averaged land evapotranspiration, and R_{land} is global-averaged river runoff. Recent studies showed that TWS plays a major role in the asymmetric ENSO-related changes in GMSL (Boening et al., 2012; Fasullo & Nerem, 2016), as a consequence of ENSO teleconnections. By analyzing the Gravity Recovery and Climate Experiment (GRACE) data and simulations from a land surface model, Ni et al. (2018) demonstrated high correlations (with maximum cross-correlation coefficients up to ~0.70) and coherence between TWS and ENSO during 2002–2015 for tropical river basins such as the Amazon and Orinoco.

ENSO shows its diversity in spatial structure and temporal evolutions (Capotondi et al., 2015; Timmermann et al., 2018). For example, the two types of warm-phase ENSO events were suggested to exist, namely, Eastern Pacific (EP) and Central Pacific (CP) types ENSO (Kao & Yu, 2009; Yeh et al., 2009). EP El Niños are generated by thermocline variations in the tropical Pacific and exhibit stronger OHC variations derived from recharge and discharge mechanisms (Jin, 1997). Whereas CP El Niños are suggested to be less involved in thermocline variations but are instead likely forced by subtropical zonal advection feedback such as the wind-evaporation-sea surface temperature feedback associated with the Pacific meridional mode (PMM) and Pacific internally driven modes (Chiang & Vimont, 2004; Min et al., 2017; Yu & Kim, 2011). Teleconnections originating from the two types of El Niños differ (Chen et al., 2016; Yeh et al., 2018; Yu et al., 2017).

Recent studies investigated the 1997–1998 (EP; see Figure 1d) and 2015–2016 (a combination of EP and CP; see Figure 1e) El Niños to better understand extreme El Niños that exhibit various forcing mechanisms and their effects (Lin & Wu, 2019; Long et al., 2020; Paek et al., 2017). Various sea surface temperature patterns among different ENSO types can excite differing wave trains, resulting in spatially varied atmospheric circulations (Paek et al., 2017), and the global water cycle (Liang et al., 2016; Xu et al., 2013). This study extends this line of work to examine the impacts of CP/EP ENSO on GMSL variation, a pioneering work to include the impacts of diverse ENSO on the interannual variations of TWS along with corresponding GMSL.

To explore the GMSL difference in 1997–1998 and 2015–2016 El Niños, we use satellite and reanalysis data sets to investigate the cause of GMSL differences between the two events, focusing on different ENSO types, and highlight the role of TWS in explaining the GMSL discrepancies observed in the two extreme events.

2. Data and Methods

We analyze satellite altimetry data using the altimeter products produced by Ssalto/Duacs and distributed by Aviso+, with support from Cnes (https://www.aviso.altimetry.fr). We use observations with global coverage for steric and barystatic heights obtained in situ Argo ocean float measurements from Scripps Institution of Oceanography (Argo, 2000; Barnoud et al., 2021; processed by the Scripps Institution of Oceanography, version: 2019) and Gravity Recovery and Climate Experiment (GRACE, RL06M; Landerer et al., 2020; Watkins et al., 2015; Wiese et al., 2016, 2018). Since the distribution of Argo is insufficient before 2004 (Leuliette & Miller, 2009) and GRACE is available only after 2002, we used reanalysis data instead to cover the steric height and TWS before 2002.

The oceanic product of Estimating the Circulation and Climate of the Ocean version 4 (ECCOv4r4; ECCO Consortium, 2020; Forget et al., 2015) is also used in this study, which contains variables for sea-level budgets and is commonly used for sea-level studies (e.g., Piecuch & Ponte, 2011; Storto et al., 2019). We analyze salinity and temperature (converted from potential temperature field) data from ECCOv4r4 to integrate ocean density from the surface to depth of 2,000 m following Equation 2 from Gill and Niller (1973) for steric variation:

$$\text{steric variation} = \frac{-1}{\rho_0}\int_{-H}^{0}\left(\rho - \overline{\rho}\right)dz, H = 2{,}000\,\text{m} \tag{2}$$

The ocean bottom pressure with global mean air pressure removed (OBPNOPAB) in ECCOv4r4 represents barystatic height. Because the runoff input in ECCOv4r4 is a fixed seasonal cycle, this might influence the oceanic water budget by freshwater inputs (precipitation, evaporation, and runoff) within ECCOv4r4. In order to deal with this issue, we use another two independent data sets covering 1993–2016: European Centre for Medium-Range Weather Forecasts (ECMWF) Reanalysis version 5-land (ERA5-land; Muñoz Sabater, 2019) and the offline Community Land Model Version 5 (CLM5; Lawrence et al., 2019) simulations, for land precipitation, evaporation, and runoff data to calculate TWS over all land areas, including Greenland and Antarctica. Assuming the TWS entering into the ocean distributes uniformly in global oceans (Farinotti et al., 2019; Jensen et al., 2013; Piexoto & Oort, 1992), we used −TWS (i.e., TWS multiplied by −1 to indicate from land into ocean) to approximate the barystatic height. For glacier-related information, water mass data for Greenland and Antarctica are obtained from RACMO2.3p2, an updated regional climate model. Outputs from RACMO2.3p2 are validated using GRACE (Noël et al., 2018; Van Wessem et al., 2018).

We employ the Oceanic Niño Index (ONI) from National Oceanic and Atmospheric Administration to characterize the strength of ENSO and the CP indices (CPI) and EP indices (EPI) to distinguish between different types of El Niño (Kao & Yu, 2009; Yu & Kim, 2010). All data sets in this study are summarized in Table S1.

We compared −TWS from ERA5-land and CLM5 to −TWS from GRACE during 2003–2016 as well as steric heights derived from Argo and ECCOv4r4 to demonstrate the veracity of model simulations. The temporal and spatial validations of ECCOv4r4 and those observations are shown and discussed in Section S1 (also see Table S2; Figures S1 and S2). ECMWF ocean and sea ice reanalysis (ORAS5; Zuo et al., 2019) are applied as independent oceanic data for consistency validation in Section S5. We bilinearly interpolate all ocean data sets (including altimetry, GRACE, and ECCO v4r4) to 1° globally in this study. The global mean of each time series is considered as area weighted and we notify readers that the definition of ocean areas vary from

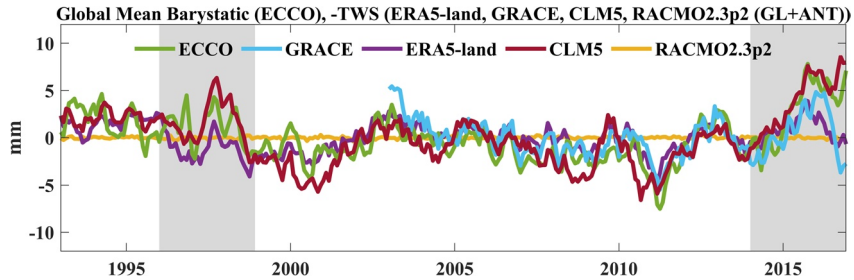

Figure 2. Time series of global mean sea level (GMSL) contributed from barystatic height from Estimating the Circulation and Climate of the Ocean version 4 (ECCOv4r4) (green line), from global mean −terrestrial water storage (TWS) from Gravity Recovery and Climate Experiment (GRACE) (blue line), from global mean −TWS from European Centre for Medium-Range Weather Forecasts Reanalysis version 5-land (ERA5-land) (purple line), from global mean −TWS from Community Land Model Version 5 (CLM5) (red line), and from Greenland and Antarctica glaciers (GL + ANT, yellow line). Gray-shaded areas denote 1996–1998 and 2014–2016 events.

data set to data set. Notably, we interpolate the missing months in GRACE data using cubic interpolation following Piecuch and Quinn (2016). Long-term linear trends (Table S3) and seasonal cycles are removed, and a 3-month running mean is applied in the time series to focus on the interannual variations of ENSO (Llovel et al., 2011) before further analysis.

3. Results

3.1. Contrasting Sea-Level Variations in 1997–1998 and 2015–2016 El Niño

Figure 1a shows a GMSL anomaly with a peak value of 9.00 mm (seasonality and linear trend during 1993–2016 removed) in January 2016 and 3.72 mm in February 1998 during the two extreme El Niño events, respectively. There is a striking difference of 5.28 ± 0.96 mm between the two events (the method for estimating uncertainties can be found in Section S2). GMSL is decomposed into steric and barystatic contributions using ECCOv4r4 data (Figures 1b and 1c). The global mean steric heights peaked during the mature phases (December–January–February in 1997–1998 and 2015–2016) of the two events. The steric variation in 1997 was greater than that in 2015 because the 1997–1998 El Niño was categorized as a typical EP El Niño that brings stronger OHC variations (Yu et al., 2017). After the ONI peak in 1998, a decrease in GMSL occurred due to the development of a strong La Niña in 1998–1999. Figures 1b and 1c also illustrate that the global mean steric variations in both cases were relatively small when compared with barystatic variations. Evidently, the distinct GMSL evolutions in the two El Niño events can be mainly attributed to barystatic variations.

3.2. From Barystatic Height to TWS Variations

We next calculate −TWS from ERA5-land to estimate the ocean mass increase in terms of land hydrological budget (Figure 2). ERA5-land reanalysis reveals that a portion of barystatic variation can be explained by −TWS with a correlation coefficient of 0.57 ($p < 0.01$, based on 1993–2016 period between ECCOv4r4 and ERA5-land) and by GRACE with a correlation coefficient of 0.67 ($p < 0.01$, based on 2003–2016 period between GRACE and ERA5-land). Furthermore, the CLM5 simulated −TWS is with 0.80 ($p < 0.01$), 0.64 ($p < 0.01$), and 0.50 ($p < 0.05$) correlation coefficients to barystatic height from ECCOv4r4, −TWS from GRACE, and −TWS from ERA5-land, respectively. The difference of −TWS (ERA5-land) in the mature phases of the two events was 2.99 ± 0.82 mm. On the other hand, the −TWS (CLM5) difference of the same time was 3.18 ± 0.86 mm, which was smaller although the peak during 2015–2016 was still higher than that during 1997–1998. We also check whether the difference of −TWS in the two events was from land ice melt from Greenland and Antarctica. With RACMO2.3p2 data set (yellow line in Figure 2), it shows that the land ice loss was not the primary cause of the observed barystatic difference in GMSL.

The increase in ocean mass was associated with the observed −TWS anomalies, indicating that more water mass was transported from land to the ocean in 2015–2016 El Niño event. Comparing the CPI and EPI for

Table 1
Correlation Coefficients (CorrCoef.), R^2, and Ordinary Least Squares Linear Regression Slopes Between Central Pacific Indices (CPI) and Eastern Pacific Indices (EPI) and Time Series of Barystatic Height From Estimating the Circulation and Climate of the Ocean Version 4 (ECCOv4r4), −Terrestrial Water Storage From European Centre for Medium-Range Weather Forecasts Reanalysis Version 5-Land (ERA5-Land), Community Land Model Version 5 (CLM5), and Gravity Recovery and Climate Experiment (GRACE)

		ECCOv4r4	ERA5-land	CLM5	GRACE
CPI	CorrCoef.	*0.45*	**0.63**	**0.56**	**0.54**
	R^2	0.20	0.40	0.32	0.29
	mm/index	1.04 ± 0.90	0.88 ± 0.33	1.50 ± 1.13	0.99 ± 0.62
EPI	CorrCoef.	0.19	−0.12	0.17	−0.01
	R^2	0.04	0.01	0.03	0.00
	mm/index	0.44 ± 1.21	−0.16 ± 0.62	0.44 ± 2.76	−0.02 ± 1.31
Time period applied		1993–2016	1993–2016	1993–2016	2003–2016

Note. The uncertainties for the regression slopes are evaluated with 90% confidence intervals by the method mentioned in Sections S3 and S4. The italicized CorrCoef. passed the Student's *t*-test with *p*-value < 0.05 and the bolded one with *p*-value < 0.01. Autocorrelations of the time series are considered when accounting for the significance test of CorrCoef.

1997–1998 and 2015–2016 El Niños, Figures 1d and 1e show that these two events have different characteristics in terms of El Niño types. Positive EPI dominantly persisted throughout 1997–1998 period with CPI near zero in contrast to CPI and EPI that evolved similarly in the 2015–2016 event. As a result, the 1997–1998 event was recognized as an EP El Niño and the 2015–2016 event was more like a mixed EP and CP El Niño (Paek et al., 2017). Therefore, in order to understand whether the different barystatic heights relate to the El Niño types, we calculate the correlation coefficients, coefficient of determination (R^2), and regression slope between CPI/EPI and global mean −TWS during 1993–2016 (Table 1; 2003–2016 for GRACE). The correlation coefficient of CPI and −TWS can be up to 0.63 ($p < 0.01$; from ERA5-land during 1993–2016), which means that the CP El Niño signature explains at most 39% of −TWS variations. Yet, the correlation coefficients of EPI and −TWS from all the products are low and did not pass the Student's *t*-test with 95% confidence level. Regression slopes of −TWS also show that −TWS increases more with CPI (can be up to 1.50 ± 1.13 mm/CPI from CLM5 during 1993–2016) than EPI.

3.3. The Spatial Distributions of TWS With CP/EP El Niño

The global mean TWS decreases further under CP Niños (i.e., larger −TWS), which contributes equivalently to increasing GMSL, but how is the spatial distribution of TWS? Figures 3a and 3b show the mean of TWS from ERA5-land during July 1997 (2015)–June 1998 (2016), respectively (Figure S3 shows the same plot as Figure 3 but using data from CLM5). The boxed regions are with lower TWS in 2015–2016. Mean TWS distribution in 1997–1998 could be explained by the regression map of TWS with EPI during 1993–2016 (Figure 3c and Figure S4 show the extended regression map as Figures 3c and 3d but for 1981–2016). However, for the mean TWS in 2015–2016, the distribution of TWS in northwestern North America and Eurasia were less interpretable with only EPI but more likely to be accounted for CPI (Figure 3d). The two regression maps suggest that the EP and CP El Niños are associated with opposite influences on interannual TWS over most boxed areas. Regions with a negative anomalous TWS, such as northwestern North America, northern South America, central and southern Africa, Australia, eastern Siberian, and western Europe, are more common in CP El Niños. The results also reflect an asymmetric global hydrological response to different types of El Niño documented in previous studies (Liang et al., 2016; Xu et al., 2013).

4. Conclusions and Discussion

The two strongest El Niños (1997–1998 and 2015–2016 events) in recent decades exhibited a similar strength in ONI, but the physical mechanisms causing both developments and their spatiotemporal features differed considerably. The 1997–1998 event was a typical EP El Niño, but the 2015–2016 event was a combination of

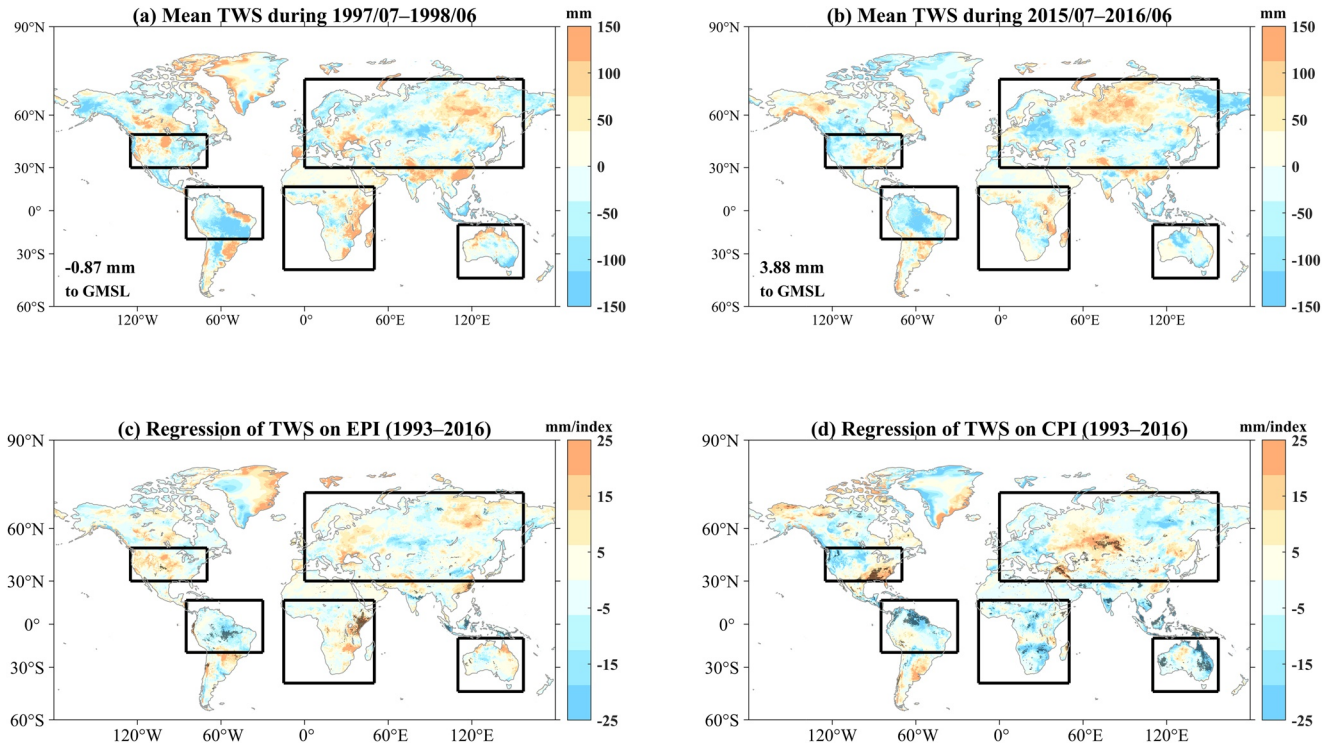

Figure 3. Mean terrestrial water storage (TWS) (European Centre for Medium-Range Weather Forecasts Reanalysis version 5-land [ERA5-land]) during (a) July 1997–June 1998 and (b) July 2015–June 2016. The numbers at the lower left corners of the panels (a and b) are the global area-weighted mean −TWS contributing to global mean sea level (GMSL) in each figure. Regression maps of (c) TWS (ERA5-land) and Eastern Pacific indices (EPI) during 1993–2016, (d) TWS (ERA5-land) and Central Pacific indices (CPI) during 1993–2016. Boxed regions are discussed in text and dotted grids passed the *F*-test with *p*-value < 0.05 for the regression slope (see Section S4).

EP and CP El Niños. These give rise to the interannual GMSL between the two events differed by approximately 5.28 ± 0.96 mm. In this study, we demonstrate that the main difference in GMSL between the two extreme El Niño events originated from barystatic components, consistent with the findings in previous studies that the ocean mass changes dominate interannual variations in sea level (Cazenave et al., 2012; Fasullo & Nerem, 2016; Llovel et al., 2011). Note that interannual variations of steric height obtained from both ECCOv4r4 and ORAS5 data (Figure S4 and Table S3) were relatively smaller than those from Argo due to varying assimilation schemes and models (Balmaseda et al., 2015; Carton et al., 2019; Storto et al., 2019). If this result is due to systematic errors in modeling procedures, the contribution of density variation in this study may be underestimated.

The barystatic variation mainly came as TWS variations, and teleconnections from CP El Niño forcing contribute more to the interannual variation of TWS, leading to the lower TWS and higher barystatic height. The regions of CP/EP ENSO-related TWS variations could be mostly explained from the precipitation patterns shown in Figure 9 of Xu et al. (2013). Several regions cannot be purely explained with only precipitation, where the evapotranspiration and runoff can be at play to modulate the net TWS variations during the CP and EP El Niños. Some diverse results from ERA5-land and CLM5 can be seen in Figures 3 and S3, and the discrepancies might come from different model resolutions, TWS schemes, and atmospheric forcings used in the two models. However, some regions (i.e., North America, central and southern Africa, Australia, Maritime Continent, and eastern Siberian) have consistent results between the two data sets. This might be also why, so far, consistent results of the global mean TWS can be seen from the two models. Further studies about model uncertainties of TWS predictability are necessary.

This study uses −TWS to represent the barystatic variations in the ocean. Here exists an uncertainty up to 1.14 mm, calculated as the standard deviation of the difference between $\Delta M_{\text{barystatic}}$ from ECCOv4r4 and $-\Delta M_{\text{land}}$ from ERA5-land throughout 1993–2016. Current land and ocean models do not consider the model-based Glacial Isostatic Adjustment signal, independent estimation of geocenter motion, and so on. The

land models may not reasonably simulate the ice melting in Greenland and Antarctica, either. Moreover, the atmospheric precipitable water is ignored in this study. These factors could also lead to uncertainties in our estimate that barystatic variation is forced by −TWS.

Previous studies have shown that the frequency of CP El Niños has increased in the early 21st century (Kao & Yu, 2009; Larkin & Harrison, 2005; Yeh et al., 2009), and future projections from climate model intercomparison projects demonstrate that the number of extreme El Niños will continue to increase (Cai et al., 2015) with more CP El Niños (Yeh et al., 2009, 2018). With the two extreme El Niños on the past records, we emphasize how the two types (CP and EP) of El Niño exhibit different teleconnections to TWS. This study makes a breakthrough in the previous view for interannual variations of GMSL excluding the El Niño complexity. Such consequent diverse responses of water redistributions on continents not only impact the temporary storage of water (i.e., terrestrial reservoirs), but also pose a danger to the coastal regions when combining with the sea level rising trend (Oppenheimer et al., 2019). Therefore, including the information of El Niño complexity and its change in the future is necessary to better understand and more accurately project future GMSL.

Data Availability Statement

The data used in this study can be obtained from ONI: https://climatedataguide.ucar.edu/climate-data/nino-sst-indices-nino-12-3-34-4-oni-and-tni; AVISO+: https://www.aviso.altimetry.fr/es/data/products/sea-surface-height-products/global/gridded-sea-level-anomalies-mean-and-climatology.html; Argo: http://sio-argo.ucsd.edu/RG_Climatology.html; GRACE/GRACE-FO Mascon data: https://grace.jpl.nasa.gov/data/get-data/jpl_global_mascons/; ECCOv4r4: https://www.ecco-group.org/products-ECCO-V4r4.htm; ORAS5: https://www.ecmwf.int/en/forecasts/dataset/ocean-reanalysis-system-5; ERA5-land: https://cds.climate.copernicus.eu/cdsapp#!/search?type=dataset&text=era5-land; information about CLM5 is in https://www.cesm.ucar.edu/models/cesm2/land/ and the model outputs from CLM5 could be accessed from the corresponding author. All the data processing and figures are done with Matlab, with the external toolbox from M_Map (https://www.eoas.ubc.ca/~rich/map.html), cpt-city (http://soliton.vm.bytemark.co.uk/pub/cpt-city/), and SEAWATER library version 3.2 is attributed to Morgan, P. P. SEAWATER: a library of MATLAB® computational routines for the properties of sea water: Version 1.2. 1994. Report No.:222. http://hdl.handle.net/102.100.100/239771?index=1. The code for this study can be accessed from Zenodo (https://doi.org/10.5281/zenodo.5144491).

Acknowledgments
This study was supported by a grant of MOST 106-2111-M-002-010-MY4 to National Taiwan University. The authors thank Dr. Lee-Lueng Fu who inspired them during this study. The altimeter products were produced by Ssalto/Duacs and distributed by Aviso +, with support from Cnes. Argo data were collected and made freely available by the International Argo Program and the national programs that contribute to it. The Argo Program is part of the Global Ocean Observing System. CPI/EPI can be reproduced following Kao and Yu (2009) and Yu and Kim (2010). GRACE/GRACE-FO Mascon data are available at http://grace.jpl.nasa.gov and https://grace.jpl.nasa.gov/data/get-data/jpl_global_mascons/.

References

Argo. (2000). *Argo float data and metadata from Global Data Assembly Centre (Argo GDAC)* (Version: 2019). SEANOE. https://doi.org/10.17882/42182

Balmaseda, M. A., Hernandez, F., Storto, A., Palmer, M. D., Alves, O., Shi, L., et al. (2015). The ocean reanalyses intercomparison project (ORA-IP). *Journal of Operational Oceanography*, *8*(Suppl. 1), s80–s97. https://doi.org/10.1080/1755876x.2015.1022329

Barnoud, A., Pfeffer, J., Guérou, A., Frery, M. L., Siméon, M., Cazenave, A., et al. (2021). Contributions of altimetry and Argo to non-closure of the global mean sea level budget since 2016. *Geophysical Research Letters*, *48*(14), e2021GL092824. https://doi.org/10.1029/2021gl092824

Boening, C., Willis, J. K., Landerer, F. W., Nerem, R. S., & Fasullo, J. (2012). The 2011 La Niña: So strong, the oceans fell. *Geophysical Research Letters*, *39*(19). https://doi.org/10.1029/2012gl053055

Cai, W., Santoso, A., Wang, G., Yeh, S. W., An, S. I., Cobb, K. M., et al. (2015). ENSO and greenhouse warming. *Nature Climate Change*, *5*(9), 849–859. https://doi.org/10.1038/nclimate2743

Capotondi, A., Wittenberg, A. T., Newman, M., Di Lorenzo, E., Yu, J. Y., Braconnot, P., et al. (2015). Understanding ENSO diversity. *Bulletin of the American Meteorological Society*, *96*(6), 921–938. https://doi.org/10.1175/bams-d-13-00117.1

Carton, J. A., Penny, S. G., & Kalnay, E. (2019). Temperature and salinity variability in the SODA3, ECCO4r3, and ORAS5 ocean reanalyses, 1993–2015. *Journal of Climate*, *32*(8), 2277–2293. https://doi.org/10.1175/jcli-d-18-0605.1

Cazenave, A., Henry, O., Munier, S., Delcroix, T., Gordon, A. L., Meyssignac, B., et al. (2012). Estimating ENSO influence on the global mean sea level, 1993–2010. *Marine Geodesy*, *35*(Suppl. 1), 82–97. https://doi.org/10.1080/01490419.2012.718209

Chen, C. C., Lin, H. W., Yu, J. Y., & Lo, M. H. (2016). The 2015 Borneo fires: What have we learned from the 1997 and 2006 El Niños? *Environmental Research Letters*, *11*(10), 104003. https://doi.org/10.1088/1748-9326/11/10/104003

Cheng, L., Abraham, J., Hausfather, Z., & Trenberth, K. E. (2019). How fast are the oceans warming. *Science*, *363*(6423), 128–129. https://doi.org/10.1126/science.aav7619

Chiang, J. C., & Vimont, D. J. (2004). Analogous Pacific and Atlantic meridional modes of tropical atmosphere–ocean variability. *Journal of Climate*, *17*(21), 4143–4158. https://doi.org/10.1175/jcli4953.1

Church, J. A., White, N. J., Konikow, L. F., Domingues, C. M., Cogley, J. G., Rignot, E., et al. (2011). Revisiting the Earth's sea-level and energy budgets from 1961 to 2008. *Geophysical Research Letters*, *38*(18). https://doi.org/10.1029/2011gl048794

ECCO Consortium, Fukumori, I., Wang, O., Fenty, I., Forget, G., Heimbach, P., & Ponte, R. M. (2020). *Synopsis of the ECCO central production global ocean and sea-ice state estimate (version 4 release 4)*. Retrieved from https://ecco.jpl.nasa.gov/drive/files/Version4/Release4

Ent, R. J., & Tuinenburg, O. A. (2017). The residence time of water in the atmosphere revisited. *Hydrology and Earth System Sciences*, *21*(2), 779–790. https://doi.org/10.5194/hess-21-779-2017

Farinotti, D., Huss, M., Fürst, J. J., Landmann, J., Machguth, H., Maussion, F., & Pandit, A. (2019). A consensus estimate for the ice thickness distribution of all glaciers on Earth. *Nature Geoscience*, *12*(3), 168–173. https://doi.org/10.1038/s41561-019-0300-3

Fasullo, J. T., & Nerem, R. S. (2016). Interannual variability in global mean sea level estimated from the CESM large and last millennium ensembles. *Water*, *8*(11), 491. https://doi.org/10.3390/w8110491

Forget, G. A. E. L., Campin, J. M., Heimbach, P., Hill, C. N., Ponte, R. M., & Wunsch, C. (2015). *ECCO version 4: An integrated framework for non-linear inverse modeling and global ocean state estimation*.

Gill, A. E., & Niller, P. P. (1973). The theory of the seasonal variability in the ocean. *Deep-Sea Research and Oceanographic Abstracts*, *20*(2), 141–177. https://doi.org/10.1016/0011-7471(73)90049-1

Gregory, J. M., White, N. J., Church, J. A., Bierkens, M. F. P., Box, J. E., Van den Broeke, M. R., et al. (2013). Twentieth-century global-mean sea level rise: Is the whole greater than the sum of the parts? *Journal of Climate*, *26*(13), 4476–4499. https://doi.org/10.1175/jcli-d-12-00319.1

Hamlington, B. D., Cheon, S. H., Piecuch, C. G., Karnauskas, K. B., Thompson, P. R., Kim, K. Y., et al. (2019). The dominant global modes of recent internal sea level variability. *Journal of Geophysical Research: Oceans*, *124*(4), 2750–2768. https://doi.org/10.1029/2018jc014635

Hamlington, B. D., Fasullo, J. T., Nerem, R. S., Kim, K. Y., & Landerer, F. W. (2019). Uncovering the pattern of forced sea level rise in the satellite altimeter record. *Geophysical Research Letters*, *46*(9), 4844–4853. https://doi.org/10.1029/2018gl081386

Hamlington, B. D., Piecuch, C. G., Reager, J. T., Chandanpurkar, H., Frederikse, T., Nerem, R. S., et al. (2020). Origin of interannual variability in global mean sea level. *Proceedings of the National Academy of Sciences*, *117*(25), 13983–13990. https://doi.org/10.1073/pnas.1922190117

Jensen, L., Rietbroek, R., & Kusche, J. (2013). Land water contribution to sea level from GRACE and Jason-1 measurements. *Journal of Geophysical Research: Oceans*, *118*(1), 212–226. https://doi.org/10.1002/jgrc.20058

Jin, F. F. (1997). An equatorial ocean recharge paradigm for ENSO. Part I: Conceptual model. *Journal of the Atmospheric Sciences*, *54*(7), 811–829. https://doi.org/10.1175/1520-0469(1997)054<0811:aeorpf>2.0.co;2

Kao, H. Y., & Yu, J. Y. (2009). Contrasting eastern-Pacific and central-Pacific types of ENSO. *Journal of Climate*, *22*(3), 615–632. https://doi.org/10.1175/2008jcli2309.1

Landerer, F. W., Flechtner, F. M., Save, H., Webb, F. H., Bandikova, T., Bertiger, W. I., et al. (2020). Extending the global mass change data record: GRACE Follow-On instrument and science data performance. *Geophysical Research Letters*, *47*(12), e2020GL088306. https://doi.org/10.1029/2020gl088306

Larkin, N. K., & Harrison, D. E. (2005). Global seasonal temperature and precipitation anomalies during El Niño autumn and winter. *Geophysical Research Letters*, *32*(16). https://doi.org/10.1029/2005gl022860

Lawrence, D. M., Fisher, R. A., Koven, C. D., Oleson, K. W., Swenson, S. C., Bonan, G., et al. (2019). The Community Land Model version 5: Description of new features, benchmarking, and impact of forcing uncertainty. *Journal of Advances in Modeling Earth Systems*, *11*(12), 4245–4287. https://doi.org/10.1029/2018ms001583

Leuliette, E. W. (2015). The balancing of the sea-level budget. *Current Climate Change Reports*, *1*(3), 185–191. https://doi.org/10.1007/s40641-015-0012-8

Leuliette, E. W., & Miller, L. (2009). Closing the sea level rise budget with altimetry, Argo, and GRACE. *Geophysical Research Letters*, *36*(4). https://doi.org/10.1029/2008gl036010

Liang, Y. C., Chou, C. C., Yu, J. Y., & Lo, M. H. (2016). Mapping the locations of asymmetric and symmetric discharge responses in global rivers to the two types of El Niño. *Environmental Research Letters*, *11*(4), 044012. https://doi.org/10.1088/1748-9326/11/4/044012

Lin, Y. F., & Wu, C. R. (2019). Distinct impacts of the 1997–98 and 2015–16 extreme El Niños on Japanese eel larval catch. *Scientific Reports*, *9*(1), 1–8. https://doi.org/10.1038/s41598-018-37569-5

Llovel, W., Becker, M., Cazenave, A., Jevrejeva, S., Alkama, R., Decharme, B., et al. (2011). Terrestrial waters and sea level variations on interannual time scale. *Global and Planetary Change*, *75*(1–2), 76–82. https://doi.org/10.1016/j.gloplacha.2010.10.008

Long, X., Widlansky, M. J., Schloesser, F., Thompson, P. R., Annamalai, H., Merrifield, M. A., & Yoon, H. (2020). Higher sea levels at Hawaii caused by strong El Niño and weak trade winds. *Journal of Climate*, *33*(8), 3037–3059. https://doi.org/10.1175/jcli-d-19-0221.1

Min, Q., Su, J., & Zhang, R. (2017). Impact of the South and North Pacific meridional modes on the El Niño–Southern Oscillation: Observational analysis and comparison. *Journal of Climate*, *30*(5), 1705–1720. https://doi.org/10.1175/jcli-d-16-0063.1

Muñoz Sabater, J. (2019). *ERA5-land monthly averaged data from 1981 to present*. Copernicus Climate Change Service (C3S) Climate Data Store (CDS). https://doi.org/10.24381/cds.68d2bb30

Nerem, R. S., Beckley, B. D., Fasullo, J. T., Hamlington, B. D., Masters, D., & Mitchum, G. T. (2018). Climate-change–driven accelerated sea-level rise detected in the altimeter era. *Proceedings of the National Academy of Sciences*, *115*(9), 2022–2025. https://doi.org/10.1073/pnas.1717312115

Nerem, R. S., Chambers, D. P., Choe, C., & Mitchum, G. T. (2010). Estimating mean sea level change from the TOPEX and Jason altimeter missions. *Marine Geodesy*, *33*(S1), 435–446. https://doi.org/10.1080/01490419.2010.491031

Ni, S., Chen, J., Wilson, C. R., Li, J., Hu, X., & Fu, R. (2018). Global terrestrial water storage changes and connections to ENSO events. *Surveys in Geophysics*, *39*(1), 1–22. https://doi.org/10.1007/s10712-017-9421-7

Noël, B., van de Berg, W. J., Van Wessem, J. M., Van Meijgaard, E., Van As, D., Lenaerts, J., et al. (2018). Modelling the climate and surface mass balance of polar ice sheets using RACMO2-Part 1: Greenland (1958-2016). *Cryosphere*, *12*(3), 811–831. https://doi.org/10.5194/tc-12-811-2018

Oppenheimer, M., Glavovic, B., Hinkel, J., van de Wal, R., Magnan, A. K., Abd-Elgawad, A., et al. (2019). *Sea level rise and implications for low lying islands, coasts and communities*.

Paek, H., Yu, J. Y., & Qian, C. (2017). Why were the 2015/2016 and 1997/1998 extreme El Niños different? *Geophysical Research Letters*, *44*(4), 1848–1856.

Peixoto, J. P., & Oort, A. H. (1992). *Physics of climate*.

Piecuch, C. G., & Ponte, R. M. (2011). Mechanisms of interannual steric sea level variability. *Geophysical Research Letters*, *38*(15). https://doi.org/10.1029/2011gl048440

Piecuch, C. G., & Quinn, K. J. (2016). El Niño, La Niña, and the global sea level budget. *Ocean Science*, *12*(6), 1165–1177. https://doi.org/10.5194/os-12-1165-2016

Storto, A., Bonaduce, A., Feng, X., & Yang, C. (2019). Steric sea level changes from ocean reanalyses at global and regional scales. *Water*, *11*(10), 1987. https://doi.org/10.3390/w11101987

Timmermann, A., An, S. I., Kug, J. S., Jin, F. F., Cai, W., Capotondi, A., et al. (2018). El Niño–southern oscillation complexity. *Nature*, *559*(7715), 535–545. https://doi.org/10.1038/s41586-018-0252-6

Van Wessem, J. M., Jan Van De Berg, W., Noël, B. P., Van Meijgaard, E., Amory, C., Birnbaum, G., et al. (2018). Modelling the climate and surface mass balance of polar ice sheets using racmo2: Part 2: Antarctica (1979-2016). *Cryosphere*, *12*(4), 1479–1498. https://doi.org/10.5194/tc-12-1479-2018

Wada, Y., Lo, M. H., Yeh, P. J. F., Reager, J. T., Famiglietti, J. S., Wu, R. J., & Tseng, Y. H. (2016). Fate of water pumped from underground and contributions to sea-level rise. *Nature Climate Change*, *6*(8), 777–780. https://doi.org/10.1038/nclimate3001

Watkins, M. M., Wiese, D. N., Yuan, D. N., Boening, C., & Landerer, F. W. (2015). Improved methods for observing Earth's time variable mass distribution with GRACE using spherical cap mascons. *Journal of Geophysical Research: Solid Earth*, *120*(4), 2648–2671. https://doi.org/10.1002/2014jb011547

Wiese, D. N., Landerer, F. W., & Watkins, M. M. (2016). Quantifying and reducing leakage errors in the JPL RL05M GRACE mascon solution. *Water Resources Research*, *52*(9), 7490–7502. https://doi.org/10.1002/2016wr019344

Wiese, D. N., Yuan, D. N., Boening, C., Landerer, F. W., & Watkins, M. M. (2018). *JPL GRACE mascon ocean, ice, and hydrology equivalent water height release 06 coastal resolution improvement (CRI) filtered version 1.0*. DAAC.

Xu, K., Zhu, C., & He, J. (2013). Two types of El Niño-related Southern Oscillation and their different impacts on global land precipitation. *Advances in Atmospheric Sciences*, *30*(6), 1743–1757. https://doi.org/10.1007/s00376-013-2272-3

Yeh, S. W., Cai, W., Min, S. K., McPhaden, M. J., Dommenget, D., Dewitte, B., et al. (2018). ENSO atmospheric teleconnections and their response to greenhouse gas forcing. *Reviews of Geophysics*, *56*(1), 185–206. https://doi.org/10.1002/2017rg000568

Yeh, S. W., Kug, J. S., Dewitte, B., Kwon, M. H., Kirtman, B. P., & Jin, F. F. (2009). El Niño in a changing climate. *Nature*, *461*(7263), 511–514. https://doi.org/10.1038/nature08316

Yu, J. Y., & Kim, S. T. (2010). Three evolution patterns of central-Pacific El Niño. *Geophysical Research Letters*, *37*(8). https://doi.org/10.1029/2010gl042810

Yu, J. Y., & Kim, S. T. (2011). Relationships between extratropical sea level pressure variations and the central Pacific and eastern Pacific types of ENSO. *Journal of Climate*, *24*(3), 708–720. https://doi.org/10.1175/2010jcli3688.1

Yu, J. Y., Wang, X., Yang, S., Paek, H., & Chen, M. (2017). *The changing El Niño–Southern Oscillation and associated climate extremes* (pp. 1–38). John Wiley & Sons, Inc. https://doi.org/10.1002/9781119068020.ch1

Zuo, H., Balmaseda, M. A., Tietsche, S., Mogensen, K., & Mayer, M. (2019). The ECMWF operational ensemble reanalysis–analysis system for ocean and sea ice: A description of the system and assessment. *Ocean Science*, *15*(3). https://doi.org/10.5194/os-15-779-2019

References From the Supporting Information

Bretherton, C. S., Widmann, M., Dymnikov, V. P., Wallace, J. M., & Bladé, I. (1999). The effective number of spatial degrees of freedom of a time-varying field. *Journal of Climate*, *12*, 1990–2009. https://doi.org/10.1175/1520-0442(1999)012<1990:tenosd>2.0.co;2

Chambers, D. P., Cazenave, A., Champollion, N., Dieng, H., Llovel, W., Forsberg, R., et al. (2017). Evaluation of the global mean sea level budget between 1993 and 2014. *Surveys in Geophysics*, *38*(1), 309–327. https://doi.org/10.1007/s10712-016-9381-3

Köhl, A., Stammer, D., & Cornuelle, B. (2007). Interannual to decadal changes in the ECCO global synthesis. *Journal of Physical Oceanography*, *37*(2), 313–337. https://doi.org/10.1175/jpo3014.1